13.3 A Mid-Infrared Imaging Spectrograph for the GMT

The wavelength range from ~3-25 μm wavelength (the thermal infrared) has sensitivities which are set by the thermal background of the sky and the telescope. The Giant Magellan Telescope, with a thermally clean optical design and adaptive optics integrated into the telescope, has the potential to be a powerful facility for infrared observations in this region. A combination of high spatial resolution and sensitivity will enable a broad range of scientific discoveries as described in the GMT science case, including the discovery and characterization of young and nearby extrasolar giant planets and the detection of debris disks down to the level of an equivalent zodiacal dust disk around other nearby solar-type stars, as well as enabling new discoveries in the fields of cosmology, galaxy evolution, and star formation.

The conceptual design and performance of a Mid-Infrared Imager and Spectrograph for the GMT (MIISE) is described below. The instrument is based on a similar concept currently being built for the Large Binocular Telescope Interferometer. The similar maximum diameter of GMT to LBT allows similar design solutions. The design includes a concept for integrating the instrument with the telescope.

13.3.1 Expected Thermal Infrared Sensitivity of the GMT

The photometric performance of a thermal infrared imager is largely set by the background emission contributed by both the optics and the sky. Using a model of the atmospheric sky brightness, we can assess the fundamental limit to a ground-based thermal infrared imager under good (precipitable water vapor of 1 mm) conditions. Figure 13.3-1 shows the expected sky brightness from the HITRAN database for a high altitude site (data originally from Gillette and Mountain 1998).

The telescope optics will contribute background emission as well. The expected level of contribution for a 5% emissive telescope is shown in Figure 13.3-1. As can be seen, an IR-optimized system is especially important for the dark portions of the spectrum at 4, 9, and 11 microns. These are expected to be important spectral regions especially for searching for giant planets and debris disks.

We can obtain an approximate photometric sensitivity of GMT if we assume the background from both the sky and telescope dominates the background. The noise, from Poisson statistics, is then set by the square root of the photon flux of this background. We can assume that the image size of point sources is set by the diffraction limit of the GMT. Using these assumptions, Table 13.3-1 shows the approximate limiting sensitivity in Janskies and Vega magnitudes for the various photometric bands covered by the MIISE.

While GMT site selection is still under discussion within the project, our experience with the MIRAC/BLINC camera at Las Campanas suggests that valuable observations can be obtained in the mid-infrared even at mid-altitude sites (Liu et al. 2003, Mamajek et al. 2004, Smith et al. 2002, 2003, Karovska 2003).

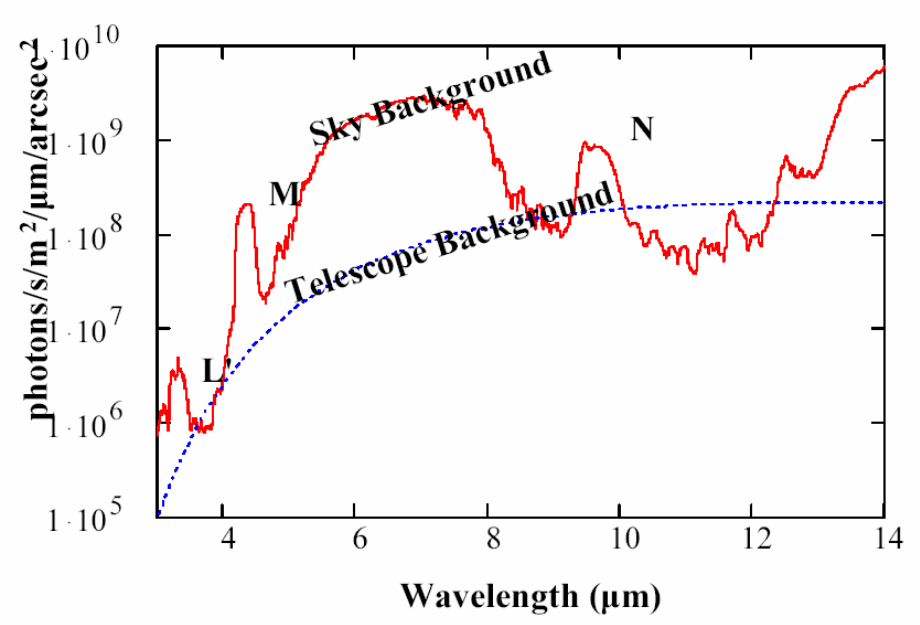

Figure 13.3-1. Expected background contribution in the thermal infrared from the sky and telescope. Atmospheric model is for a high altitude site with PWV of 1 mm (originally from Gillette and Mountain 1998).

Table 13.3-1

Photometric Performance and AO-corrected field of view for the MIISE.			
Band	**1 hour, 5σ detection limit**		**Isoplanatic Patch**
	μJy	**Vega magnitude**	**arcseconds**
K (2.2 μm)	**0.017**	**26.4**	**20**
L' (3.8 μm)	**0.49**	**21.9**	**38**
M (4.8 μm)	**5.14**	**18.7**	**51**
N (10.6 μm)	**20**	**15.7**	**132**
Q (18.0 μm)	**100**		**249**

13.3.2 Instrument Requirements

We expect the design of the thermal infrared camera to be an iterative process. Coupled with adaptive optics, the long wavelength allows a diffraction-limited field which could be quite large (see Table 13.3-1). How much of this field is covered depends on the scientific return for the larger fields, as well as the expected detector format available for the various wavelengths. While the scientific return is at least partially understood, and drives us towards at least 30″, the

changing state of infrared detector technology makes the prediction of available detector format uncertain over the timescale expected for completing the GMT.

Thermal-infrared imaging with the GMT will allow the study of the transition of disks to planets as discussed in the science case. Spatially-extended debris disks (e.g. beta Pic, HR 4796, and perhaps with the GMT, Fomalhaut) require fields of view from a few to tens of arcseconds from 8-25 μm. Because of the dependence of grain temperature on radius, it is usually best to attempt resolving a circumstellar disk at the wavelength of the coolest emission (longest wavelength) possible. The faintness of these disks compared to their star will favor the use of nulling interferometry. The GMT is well suited for these observations. Individual segments can be interfered to probe for faint extended structure at various orientations and spatial extent. The baseline between pairs of segments will allow the detection of dust as close as approximately 0.6 AU for a star at 10 pc. This is an interesting region, providing the capability to probe the habitable zones around many nearby stars.

Observing the collapse of molecular clouds to form stars and planets also requires multi-color infrared imaging. Collapsing protostellar cores are often found in groups that evolve into embedded stellar clusters where most stars are thought to form. Protoclusters containing dozens of targets typically span fields greater than 30 arcseconds and are best studied at wavelengths from 3-25 μm. Figure 13.3-2 shows an example of such a cluster that is being studied with the IRAC camera on the Spitzer Space Telescope. The GMT would have 30 times the spatial resolution and be able to zoom into the embedded heart of this forming protocluster.

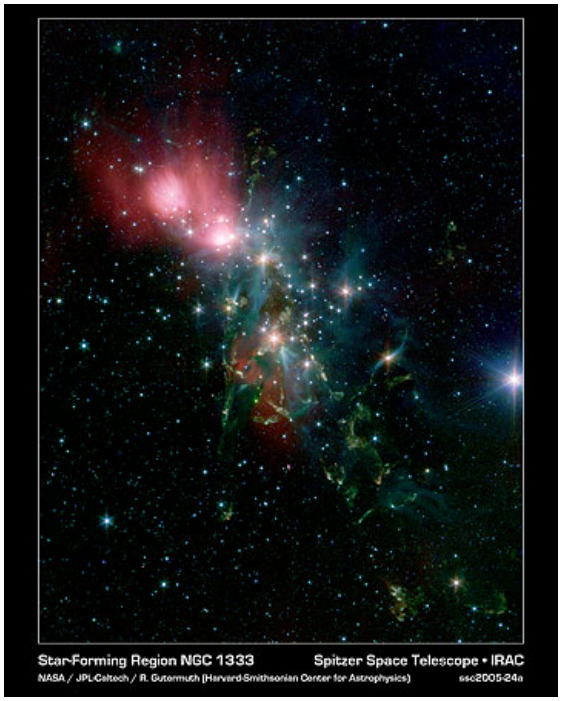

Figure 13.3-2. The embedded star cluster NGC 1333 from Spitzer, showing a 26x34 arcminute region. With 30 times the resolution, GMT could study embedded star formation in the dense core regions of these clouds.

Spectral resolutions greater than 1000 are required in order to separate important features in the mid-IR spectra of protostars and debris disks. Examples include distinguishing PAH emission from silicate dust, determining the fraction of amorphous and crystalline grains, and distinguishing various gas species in absorption for deeply embedded protostars. ISO observations of the embedded protostar W33a (see Figure 13.3-3) indicate a rich chemistry in the circumstellar environment resolvable with R > 1500. The ability to spatially resolve these spectra through long-slit spectroscopy will also permit full investigation of the interaction of a forming protostar with its environment such as HH46/47 in Figure 13.3-3 The mid IR imaging spectrograph for the GMT will have similar spectral resolution to these examples from Spitzer combined with exquisite spatial resolution.

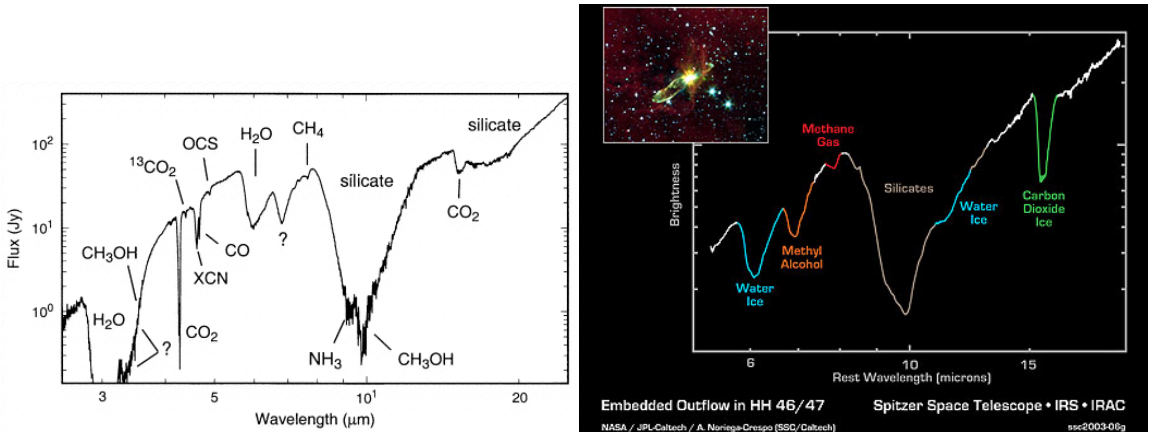

Figure 13.3-3. Example spectra from Spitzer observations. The right spectrum is W33a; the left spectrum is HH46/47. Resolutions of 1500 allow compositional studies of protostars and disks at the dramatically improved spatial resolution of the GMT.

The GMT will have the capability to detect younger or more massive giant planets. A favorable portion of the spectrum for this detection is the L′ and M band atmospheric windows. Models of gas giant planets, as well as Jupiter itself, exhibit an anomalous peak in emission around 5 microns, due to the lack of absorption features in this part of the spectrum. We expect that the optimal detection approach for these observations will combine precision adaptive optics and coronagraphic techniques to allow high dynamic range detection.

Due to detector technology, the natural approach to fulfilling the wavelength range and modes of operation, is to have two independent channels. The short wavelength channel will cover 3-5 μm observations. In addition to imaging and low resolution spectroscopy, coronagraphic techniques will be implemented in this channel to optimize the GMT for giant planet detection and characterization. The long wavelength channel will allow observations over 8-25 μm. Imaging and low resolution spectroscopy, either with or without using nulling interferometry will be possible.

Based on the above science drivers we adopt the requirements below for the MIISE (Table 13.3-2).

Table 13.3-2. MIISE Requirements.

Parameter	Requirement
Field of View	30-50″
Wavelength Range	3-25 microns
Spectral Resolution	1500
Modes	Imaging, Spectroscopy, Coronagraphy, Nulling

13.3.3 Instrument Design

The concept for the GMT Mid Infrared Imager and Spectragraph (MIISE) is based on modifying the existing camera design for the LBTI to suit the geometry of the GMT. The similar edge-to-edge spacing of the LBT and the GMT make the LBT Thermal Infrared Imager a natural starting point.

13.3.3.1 Detector Choice

The choice of detectors for the MIISE will likely change from the conceptual design based on improved fabrication capabilities from current expectations. The likely best detectors currently foreseen at 3-5 μm are HAWAII-2RG detectors. These are MBE-grown Mercury Cadmium Telluride (HgCdTe) devices with integrated 32 channel readouts. The readouts can be clocked as fast as 5 MHz per pixel, allowing full frame reads as fast as 26 ms, for high background conditions. The detectors are manufactured by Rockwell with an 18 μm pixel pitch in formats of 2048x2048. The detectors are suitable for creating a 2x2 mosaic.

State of the art for longer wavelength detectors is likely to be based on the MegaMIR project, a development lead by a group at JPL. The detectors are based upon Arsenic doped Silicon material with an integrated 16 channel readout. The current generation of detectors is fabricated by DRS Technologies in a 256x256 format as well as Raytheon in a 320x240 format. The detectors have good quantum efficiency from 5-25 μm. The MegaMIR detectors have a pixel pitch of 18 μm in formats of 1024x1024. While testing and final characterization is still underway, the detectors are being designed with suitably high well depth and fast readouts to allow efficient observing under the high background conditions of ground-based observing.

In addition to the science detectors, a near-infrared phase detection sensor is used to control the nulling interferometer phase. It is expected that a small portion of a HAWAII-2 detector could be used to achieve this phase sensing, though lower-noise alternatives may be available on the timescale of GMT.

13.3.3.2 Camera Plate Scale

The diffraction-limited point spread function (PSF) width for the GMT at 3 μm is 25 mas per pixel. For the short wavelength channel, we choose a plate scale of 10 mas per pixel. This requires a final focal ratio of f/5 at the detector. To fulfill the requirements for field of view, we plan a 2x2 mosaic of HAWAII-2RG detectors, resulting in a 40 arcsec FOV for the short wavelength channel.

The PSF for the GMT at 8 μm is 66 mas per pixel. For the long wavelength channel we choose a plate scale of 30 mas per pixel. This requires a final focal ratio of f/15 at the detector. A single MegaMIR detector will allow a 30 arcsec FOV. This is closely matched to the FOV for the short wavelength channel.

13.3.3.3 Modes of Operation

The MIISE design is intended to allow for a range of observing approaches. We can divide these approaches into an optics mode (standard imaging, nulling interferometry, and coronagraphic imaging) and wavelength mode (imaging or spectroscopy). The design approach of the MIISE is to allow use of either choice of wavelength modes to use in combination with the choice of optics mode. Table 13.3-3 shows the various observing modes possible with the MIISE. Note that we are not planning coronagraphy for the long wavelength channel, nor nulling interferometry for the short wavelength channel, since each approach to high dynamic range is better suited towards its respective wavelength range. A goal of the design is to allow simultaneous imaging at 3-5 μm and 8-25 μm. This may allow more efficient use of long exposures, for example, being able to look for debris disks at 11 μm and giant planets at 5 μm simultaneously.

Table 13.3-3

Operational modes for the MIISE				
Optics Mode	**Wavelength Mode**	**λ (μm)**	**Field**	**Focal ratio**
Standard	Imaging	3-5	40″	f/5
	Spectroscopy	3-5		f/5
	Imaging	8-25	30″	f/15
	Spectroscopy	8-25		f/15
Coronagraphy	Imaging	3-5	40″	f/5
	Spectroscopy	3-5		f/5
Nulling	Imaging	8-25	30″	f/15
	Spectroscopy	8-25		f/15

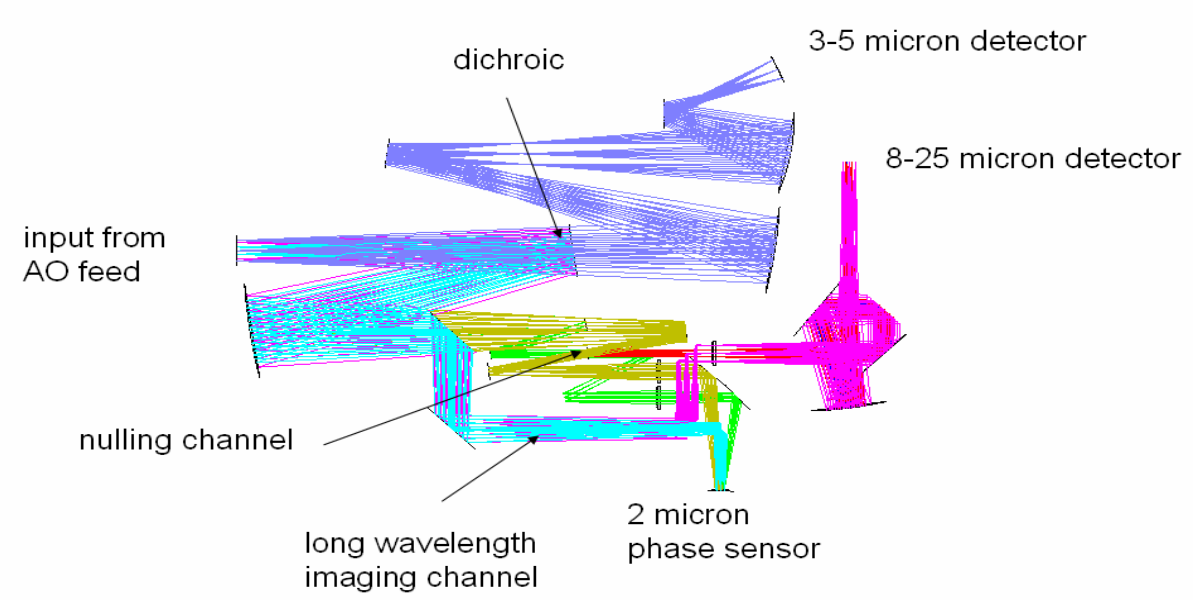

Figure 13.3-4. Conceptual optical design for the MIISE. The SWC is comprised of the grey-blue beams at the top. The LWC forms the bottom and right portion of the design. The overall scale of the drawing is approximately 1 meter width by 0.75 meter high.

13.3.3.4 Optical Design

The optical design for the GMT Thermal Imager is based on the camera portion of the Large Binocular Telescope Interferometer. Reflective optics are used to reimage the f/8 Gregorian focal plane that is folded to the camera via an external dichroic. The optical design is shown in Figure 13.3-4. The design can be split into the Short Wavelength Channel (SWC) and the Long Wavelength Channel (LWC). The left side of the image shows the folded Gregorian focal plane of the telescope. Light diverges from this point and is split by a user-selectable dichroic into the SWC, occupying the top portion of the ray trace in Figure 13.3-4 and the LWC, which occupies the bottom and right side of the drawing in Figure 13.3-4. The use of a user selectable dichroic will allow all of the light to be sent to either the SWC or the LWC for optimum throughput.

The Short Wavelength Channel (3-5 μm): Light transmitted through the dichroic (the grey-blue beams) is reimaged using a biconic mirror to form an intermediate focal plane. Coronagraphic field stops as well as slits will be placed at this plane. The light then is folded by a flat mirror and diverges to a second biconic mirror which reimages the f/8 beam to a focal ratio of f/5. A final fold mirror directs the light toward the detector. Just after the final fold an image of the telescope pupil is formed. This portion will be used to place coronagraphic masks and phase plates, as well as filters and grisms for the wavelength selection.

Biconic mirrors (optics defined by a different radius of curvature and conic constant along the two orthogonal axes of the optic) are difficult to manufacture using standard polishing techniques. However, diamond turning of aluminum mirrors has proven to be a successful technique in fabricating these shapes, and is now a common practice for companies such as II-VI Inc. The use of such optics allows reflective designs which are unobscured and relatively

compact compared to more standard approaches. The design shown for the SWC in Figure 13.3-4 uses two such devices, matched in a way similar to a two element off-axis parabola system, such that the aberrations from an off-axis source for one optic is compensated for by using the second biconic. The advantage of this approach is the achromatic nature of the design coupled with its relatively compact design. In addition the intermediate image and pupil planes are available making the design well suited for use as a coronagraph. **Error! Reference source not found.** shows the image quality of the current design. The largest biconic mirror has a diameter of 140 mm, easily within the manufacturing limit of diamond turning machines. Typical figure errors are λ/4 at optical wavelengths, and surface roughness of 50 Angstroms. We expect to study the effect of these tolerances on the design as it is refined. Tighter tolerances may be required for high contrast imaging, but these will not degrade the image quality for standard imaging or spectroscopy.

The coronagraph in the short wavelength channel will likely be a phase plate which can suppress the diffraction on one side of the star. However, we expect the best approaches to ground-based coronagraphy to be refined over the timescale of GMT fabrication. It is likely that the current design, by having an accessible image and pupil plane can accommodate a range of coronagraphic techniques. For example, the size of the intermediate 40″ focal plane is 38 mm, or approximately 60 μm diameter for a 2 λ/D occulting spot. The size of the intermediate pupil plane is 15 mm.

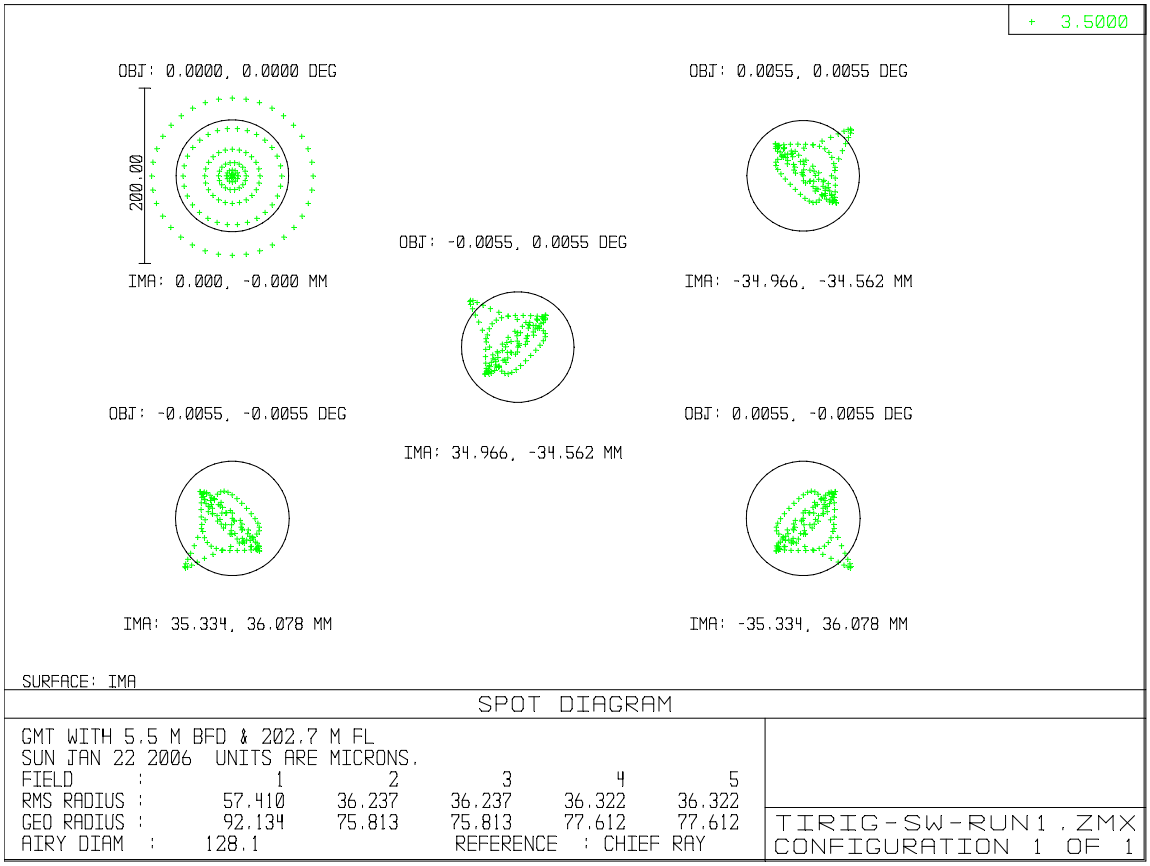

Figure 13.3-5. Spot Diagrams for the SWC at the center and corners of a 40 arcsecond field of view. The circles show the diffraction limit at 3.5 μm wavelength. Further optimization may be necessary, but the current concept already shows images with >85% Strehl for the SWC.

The Long Wavelength Channel (8-25 µm)

Light reflected from the first dichroic is reimaged by the LWC and sent to either an imaging channel or a nulling interferometer. The channel in use then illuminates the camera for the LWC, shown on the right side of Figure 13.3-4 (the pink beams). The short wavelength light is diverted prior to the camera optics toward a 2 micron phase sensor. This allows the nulling interferometer to sense and correct phase variations by using the interfered shorter wavelength light which has followed the exact same path as the mid infrared light. The optical approach in the LWC is nearly identical to the SWC. Two biconic mirrors are used to create intermediate pupil and image planes. In this case the second biconic reimages the f/8 to create a final beam with a focal ratio of f/15. Image quality for the current design is shown in Figure 13.3-6. An intermediate image plane right before the camera optics allows the insertion of slits for grism spectroscopy.

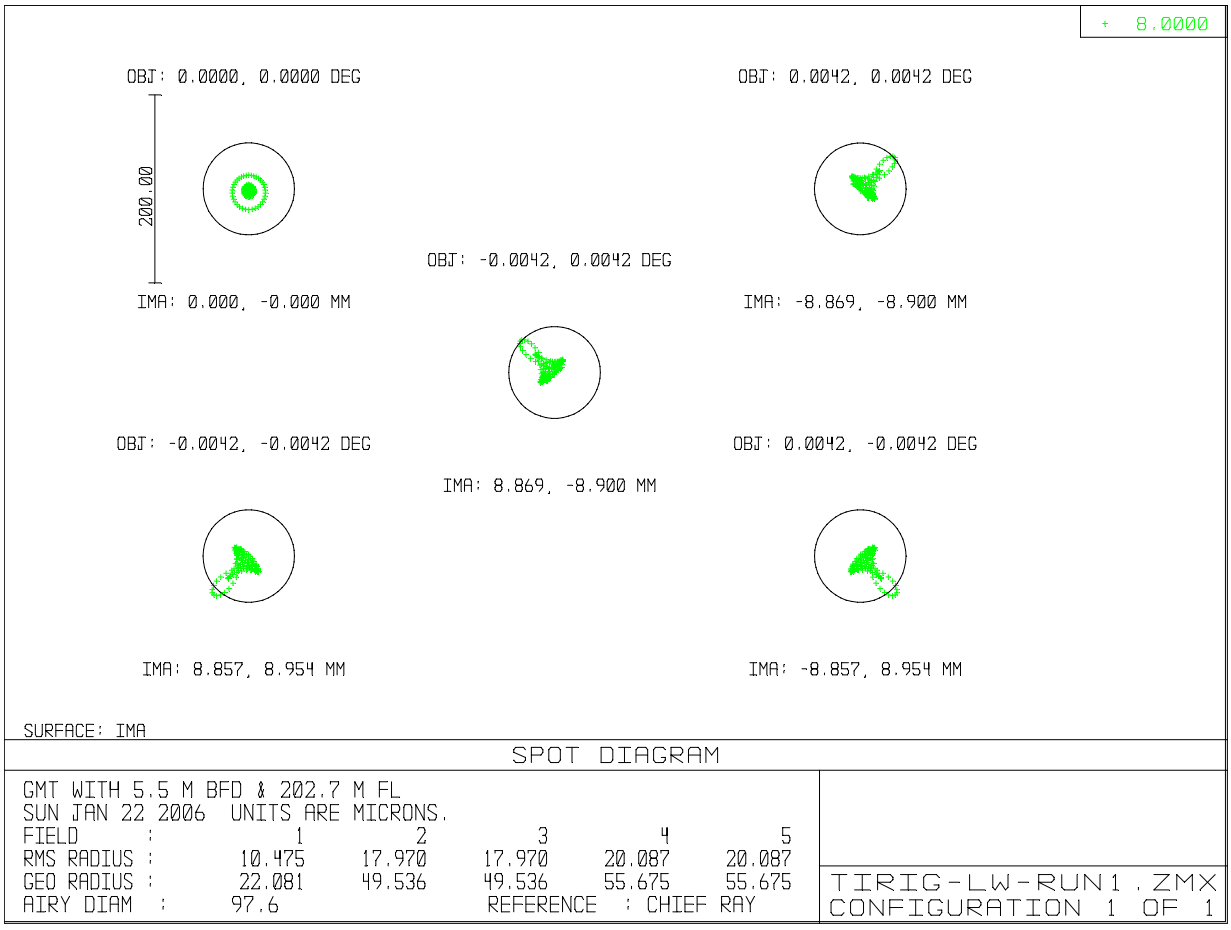

Figure 13.3-6. The point spread functions for the long wavelength channel (LWC) at 8 µm at the center and corners of a 30 arcsecond FOV. The width of the image is within the diffraction limit and corresponds to approximately 93% Strehl.

Nulling interferometry will be more complex with the GMT due to the multiple apertures. The current plan is to combine the segments across from each other to obtain measurements of disk structure over a range of orientations. It is not clear at the moment whether this will provide the

best approach to characterizing debris disks around nearby stars. We expect that further design of the MIISE will address this issue and explore, for example, the complexity and advantage of combining all different combinations of the segments in a nulling interferometer.

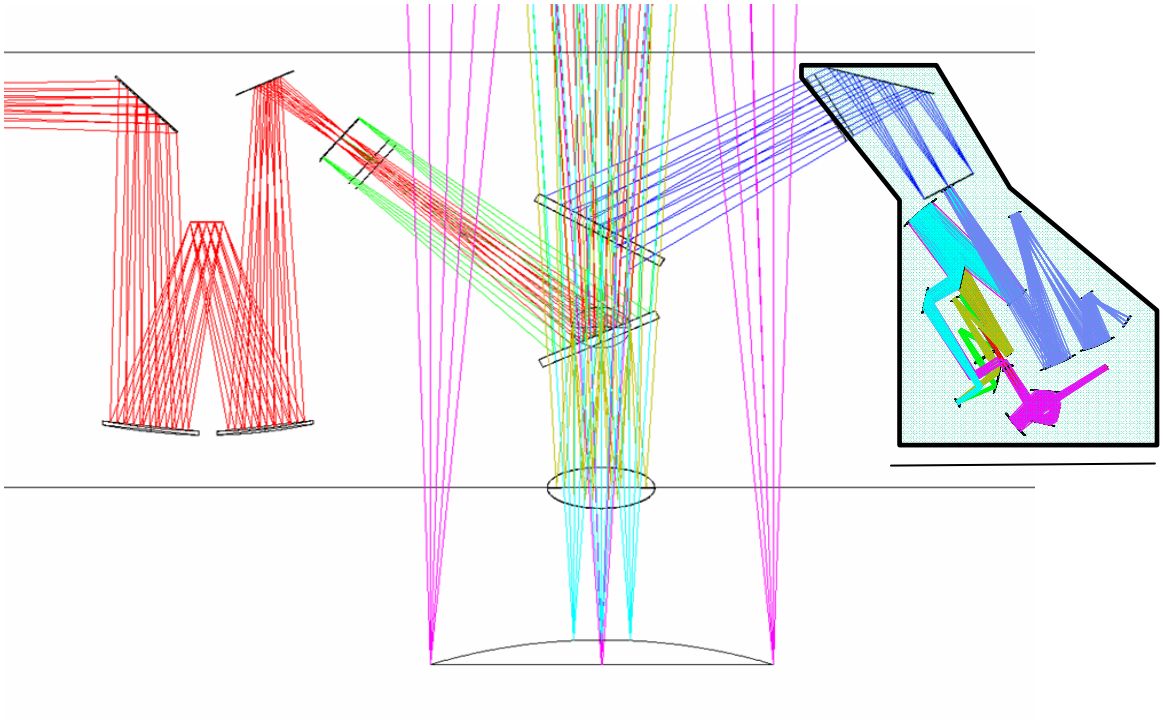

Figure 13.3-7. The MIISE in the GMT. A dichroic feeds light longer than 2 microns to the MIISE (the blue rays in the diagram). A four arcminute field of view is shown from the telescope. The MIISE design currently uses a small portion of this. The design could be updated should larger format detectors become feasible on the time scale of the GMT. The MIISE is clear of the wide field rays (the pink rays) allowing it to be installed without removal while other instruments are in use. Near-infrared light is transmitted to the station on the left (the red rays) to allow wavefront sensing.

13.3.3.5 Mechanical Design

Figure 13.3-7 shows the conceptual size for the MIISE. The instrument is housed in a single large cryostat enclosing all of the optics after the dichroic fold flat. The fold flat directs the beam upwards at an angle of 30 degrees. An entrance window placed outside the radius of the field of view needed for the wide field GMT instrumentation allows all subsequent optics to be cooled. An additional fold flat places the Gregorian focus at the top edge of the instrument. A trapezoidal enclosure approximately 1.3 m wide by 0.3 m in depth houses the optics and detectors. Figure 13.3-8 shows the expected placement of the MIISE on the GMT instrument platform. The instrument will mount to the platform below and will not need to be moved when other instruments are in use.

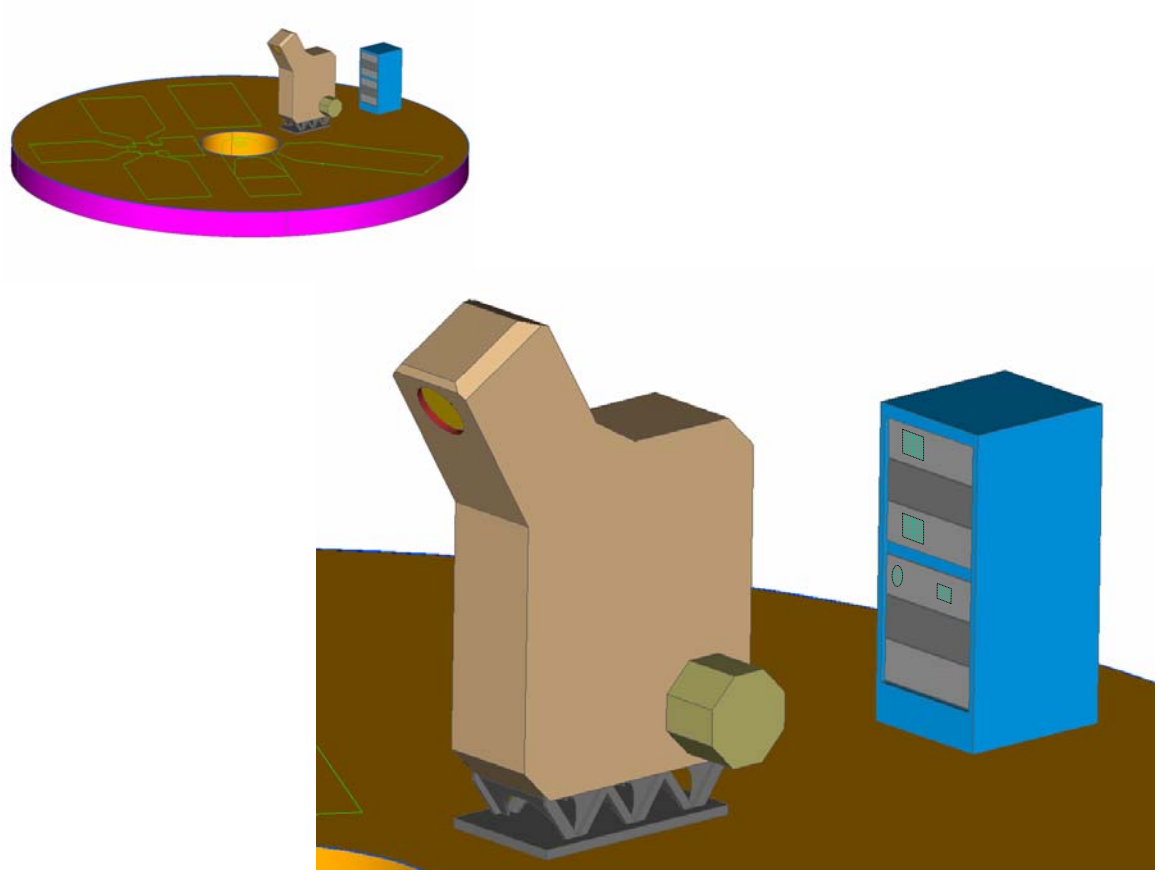

Figure 13.3-8. The MIISE on the GMT instrument platform. The down-looking entrance window accepts the telescope beam from a dichroic mirror. The instrument is shown attached to the platform below it.

13.3.3.6 Cryogenic Design

Cooling of the instrument reduces the background emission of the optics, but also is important for minimizing the dark current of these long wavelength detectors. The temperature needed is mainly set by the latter. The strictest constraints are set by spectroscopy. From Figure 13.3-1, above, we can estimate that at 4 μm a flux of approximately 10^6 photons/m^2/s/μm/arcsec^2 are incident on the GMT. Using 10 mas pixels and the collecting area of the GMT we can estimate a background photon flux of 36,000 photons per second per μm. For an R=2000 spectrum the bandwidth is 0.002 μm, giving a background of approximately 72 photons per second. For the short wavelength channel dark current is expected to be below 1 electron per second for temperatures of 60 K. At long wavelengths the darkest region at 11 μm has a background of approximately 10^8 photons/m^2/s/μm/arcsec^2, or, for the 0.03 mas pixels, $4x10^7$ photons per second per μm. For an R=2000 spectrum this is a background of $2x10^5$ photons per second. We expect that dark current can be reduced to 3000 electrons per second for the long wavelength channel at a temperature of 6 K, based on performance of current generation Arsenic-Doped Silicon detectors.

A natural solution to the two different operating temperatures needed is to use a two stage mechanical cooler. Most of the instrument will be cooled to ~60 K, including the short wavelength detector. The second stage cooler will be used to cool just the Si:As array to ~6-8 K and optics to allow background limited performance with this detector, as shown in Figure 13.3-9.

The baseline for cooling is a dual stage pulse tube cooler capable of 4 K operation. The pulse tube cooler is preferable to other more standard closed cycle systems due to its low vibrations. Using the approximate size of the first and second stage cooled volumes, the estimated radiative heat load is 70 W at 60 K for the first stage and 0.2 W at 6 K for the second stage. The Cryomech PT-410 cooler is the most common pulse tube cooler currently in operation.
It can provide 80 W of cooling at 60 K, and 1 W of cooling at 4 K.

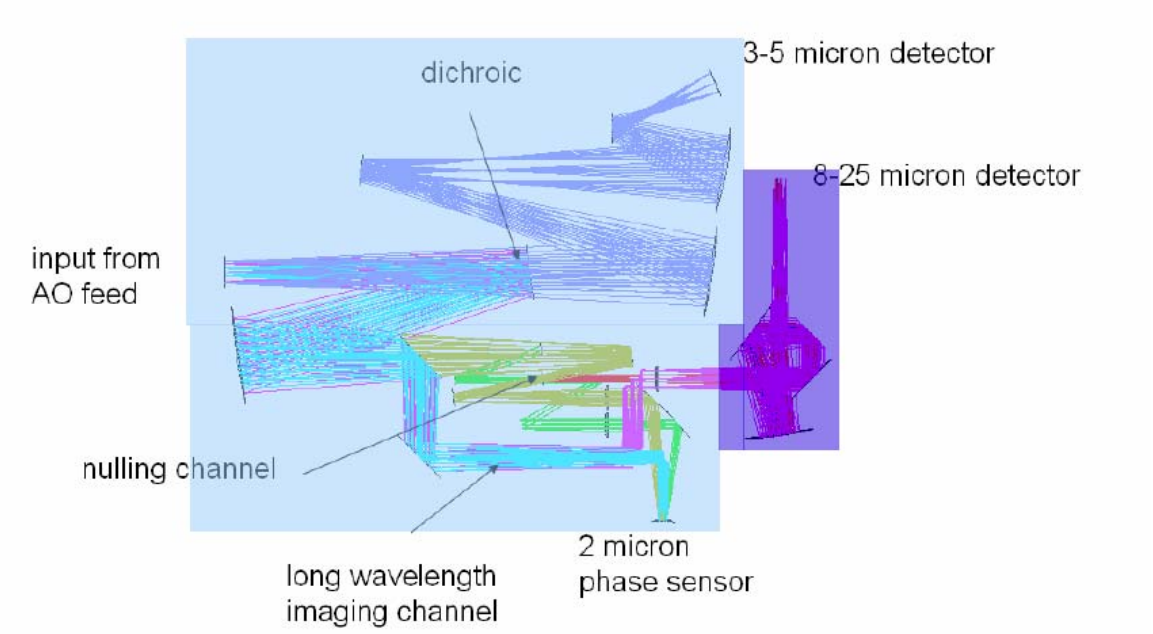

Figure 13.3-9. Cryogenic volume for the MIISE. A two stage cooler will be used to cool the cryostat. The light blue would be cooled to approximately 60 K, and the dark blue would be cooled to 6 K. Thermal calculations indicate that a Cryomech PT-410 cooler could handle the thermal load for the complete system.

13.3.3.7 Electronics Design

The instrument will be comprised of three sets of readout electronics for the short wavelength detectors, the long wavelength detector, and the near-infrared phase sensor.

The readout speed and noise characteristics required for the operation of these detectors are within the range of current readout electronics.

Various actuators will be needed for filter changes, optical alignment and mode changes within the instrument. Based on the LBTI design, we anticipate approximately twenty motors needed.

Cryogenic actuators would not be needed for any of the movements, thus these motors will likely be commercial stepper motors.

Various diagnostic and monitoring sensors for vacuum and temperature will be integrated into the instrument. These will allow temperature stabilization of the detectors and provide for health monitoring of the instrument.

13.3.3.8 Telescope and Adaptive Optics Interface

The MIISE is designed to take advantage of the integrated adaptive optics in the GMT design. The fold dichroic transmits light shortward of 2 μm while reflecting the infrared light into the MIISE. This approach allows visible light wavefront sensing using a common system capable of both natural guide star and laser tomography adaptive optics. Phase sensing between the apertures will be carried out in the near infrared either within the thermal imager (as in the LBT design) or sent to a general purpose device which can be shared with near-infrared instruments.

The expected performance of the GMT adaptive optics will deliver images which at 4 μm wavelength provide >90% Strehl longward of 4 microns. Thus high dynamic range imaging will be possible with the thermal imager without the need for additional deformable elements.

13.3.4 References

Gillett, F.C. & Mountain, M. 1998, *ASP Conf. Ser.* **133**, p. 42.

Karovska, M.; Marengo, M.; Elvis, M.; Fazio, G. G.; Hora, J. L.; Hinz, P M.; Hoffmann, W. F.; Meyer, M.; Mamajek, E. 2003, **ApJ** 598, 91.

Liu, W. M.; Hinz, P. M.; Meyer, M. R.; Mamajek, E. E.; Hoffmann, W. F.; Hora, J. L. 2003, **ApJ** 598, 111.

Mamajek, E. E.; Meyer, M. R.; Hinz, P. M.; Hoffmann, W. F.; Cohen, M.; Hora, J. L. 2004, **ApJ** 612, 496.

Smith, N.; Gehrz, R. D.; Hinz, P. M.; Hoffmann, W. F.; Mamajek, E. E.; Meyer, M. R.; Hora, J. L. 2002, **ApJ** 567, 77.

Smith, N.; Gehrz, R. D.; Hinz, P. M.; Hoffmann, W. F.; Hora, J. L.; Mamajek, E. E.; Meyer, M. R. 2003, **AJ** 125,1458